

Upgrading Quantum Metrology by Combined Sensitivity Resources in Mixed Linear-Nonlinear Light-Matter Interactions with Bias Field

Zu-Jian Ying^{1,2,*}

¹*School of Physical Science and Technology, Lanzhou University, Lanzhou 730000, China*

²*Key Laboratory for Quantum Theory and Applications of MoE, Lanzhou Center for Theoretical Physics, Lanzhou University, Lanzhou 730000, China*

The major goal of quantum metrology (QM) is to exploit the quantum resources to raise the measurement precision (MP) as high as possible. When the quantum resources such as squeezing has been widely explored, light-matter interaction systems set up a highly controllable platform applicable for QM in novel pursuit of high MP. However, critical QM by the conventional linear interaction is confronted with the restriction of low-frequency-limit condition and the detrimental problem of diverging preparation time of the probe state (PTPS). This work shows that mixed interactions by linear and nonlinear light-matter couplings in the presence of bias field can provide various quantum resources, including squeezing, degeneracy lifting, displacement and quantum phase transition. These resources manifest high sensitivity for QM as demonstrated by analytically obtained critical components or exponential behavior of quantum Fisher information. We find that these sensitivity resources can be combined to upgrade the upper bound of MP by many orders over the widely-applied squeezing resource. As further advantages, such an upgraded metrology protocol not only breaks the frequency-limit restrictions but also avoids the detrimental problem of diverging PTPS which were both encountered in linear interaction. Our work paves a way to exploit and combine all the resources in momentum, position and spin spaces to maximize the MP and expand the applicable conditions simultaneously.

PACS numbers:

I. INTRODUCTION

Recently increasing efforts have been exerted on the development of quantum metrology (QM) which is a cornerstone of quantum technologies [1–11]. On the other hand, with high controllability and tunability light-matter interactions [12–18] are building an ideal platform with great potential for applications in QM [1, 4–7, 11].

The main quantum resources widely applied for QM [19] include entanglement [20] and squeezing [21–25]. Entanglement as a QM resource suffers from the difficulties of producing and maintaining due to its vulnerability [26] and also its detection is often complex and challenging [27]. Squeezing, with its robustness to decoherence and dissipation, has been mostly explored in QM [21–25]. Since essentially the major aim of QM is to exploit the quantum resources to realize the measurement precision (MP) as high as possible, it is still desirable to explore novel quantum resources or approaches to attain higher measurement precision. In this regards, critical QM is arising to open a promising avenue for QM by exploiting the sensitivity in the critical behavior of quantum phase transition (QPT) [1, 4–7]. It is worthy to note that QPT is not an exclusive phenomenon of thermodynamical systems in condensed matter, actually in recent years it has been found that finite-component systems in light-matter interactions can also manifest QPTs [11, 28–49]. Indeed, the fundamental model in lighter-matter interactions—the quantum

Rabi model [14, 50–52]—possesses a QPT with the low-frequency limit as a replacement of the thermodynamical limit in condense matter [29–31, 33, 34]. In fact, these two limit can be even bridged via critical scaling relation [34]. As the coupling in the quantum Rabi model is linear, the critical QM based on the quantum Rabi model can be referred to as linear critical QM here.

Although the finite-component systems are not bothered by the difficulty to reach a strict thermodynamical equilibrium required by the high precision in QM of many-body systems, linear critical QM is however confronted with some other problems. These problems include limitation of the transition to a single parameter point, requirement of the low-frequency limit, and diverging preparation time of probe state (PTPT) [1, 6, 55], which might hinder the applications of linear critical QM. Improved protocols of critical QM surmounting these problems are in need.

Nevertheless, in the emerging phenomenology of light-matter interactions [11–18, 28–75] finite-component QPTs can exhibit abundant exotic quantum phenomena such as criticality and universality [29–34, 37, 39], multicriticality [35–39, 41, 49, 76, 77], compromise of universality and diversity [37, 39], topological phase transitions conventionally with [37–39] and unconventionally without [38–41] gap closing, anti-level-crossing and spin knot states [40], coexistence of Landau-class and topological-class transitions [11, 37, 39, 41], robust topological feature against non-Hermiticity [42] and universal criticality of exceptional points [11]. In particular, the nonlinear interaction manifests various patterns of symmetry breaking which lead to different types of QPTs [35, 36]. These

* yingzj@lzu.edu.cn

exotic properties might provide more potential quantum resources for QM.

In the present work, we propose to explore and combine various sensitivity resources to upgrade the upper bound of measurement precision in QM. Such a protocol can be realized in a light-matter-interaction system with mixed linear and nonlinear couplings in the presence of bias field. Indeed, from the system we extract several quantum resources, including squeezing, degeneracy lifting, displacement and QPT, all with high sensitivity. We analytically obtain the critical components or exponential behavior of QFI which represents the upper bound of measurement precision. We combine and compare these resources step by step, showing that each combination can give a dramatic boost to the enhancement of the QFI. Finally a broadest combination of squeezing, displacement and QPT yields a maximized QFI with an improvement by many orders over the widely-used squeezing resource. Besides the upgrading of the upper bound of measurement precision, our protocol of QM also shows several other advantages including more global parameter regime, breaking the frequency-limit restriction, and avoiding the detrimental diverging PTPS which were all encountered as problems in linear critical QM. By a more general view in the Wigner function, our work paves a way to exploit and combine all the resources in momentum, position and spin spaces to upgrade the measurement precision and simultaneously expand the applicable regime and conditions.

The paper is organized as follows. Section II introduces and reformulates the light-matter interaction model with mixed linear and nonlinear couplings in the presence of bias field. Section III defines and simplifies the QFI which characterizes the upper bound of measurement precision in QM. Section IV describes different variation patterns of the wave function which provide various sensitivity resources for QM. Section V is devoted to combinations of different sensitivity resources to upgrade the measurement precision in QM, eventually with enhancement of QFI by many orders. Section VI shows several more advantages of our QM protocol in extending parameter application regime, breaking the frequency-limit restriction, and avoiding divergent PTPS. Section VII analyzes the resources by the Wigner function to gain a more general view from the position, momentum and spin spaces. Finally, Section VIII gives a summary of conclusions.

II. ASYMMETRIC LINEAR-NONLINEAR-MIXED QUANTUM RABI MODEL

We consider a general nonlinear quantum Rabi model for light-matter interactions [36]

$$H = \omega a^\dagger a + \frac{\Omega}{2} \hat{\sigma}_x + g_1 \hat{\sigma}_z (a^\dagger + a) + g_2 \hat{\sigma}_z (a^\dagger + a)^2 - \epsilon \hat{\sigma}_z. \quad (1)$$

which describes couplings between a quantized bosonic mode with frequency ω , created (annihilated) by a^\dagger (a), and a qubit represented by the Pauli matrices $\hat{\sigma}_{x,y,z}$. Here Ω denotes the energy splitting of atom in cavity system and the tunneling or spin flipping energy of flux qubit in superconducting circuit system [78]. The interactions include the conventional linear coupling with strength g_1 [14, 50–52] and a nonlinear coupling with strength g_2 [79–85]. The physical regime of g_2 lies in $[0, g_T]$, while beyond the spectral collapse point g_T the system is unstable without lower energy bound [79–84]. Here the spectral collapse point of g_2 has shifted from $g_t = \omega/2$ in the two-photon coupling $\hat{\sigma}_z [(a^\dagger)^2 + a^2]$ to $g_T = \omega/4$ in the full quadratic coupling $\hat{\sigma}_z (a^\dagger + a)^2$ [35, 36]. Finally in H , the ϵ term is the bias field which can be tuned by external flux in superconducting circuit systems.

The linear quantum Rabi model has the symmetry $P_1 = \hat{\sigma}_x e^{i\pi a^\dagger a}$. Differently the nonlinear coupling in the two-photon form possesses the symmetry $P_2 = \hat{\sigma}_x e^{i\pi a^\dagger a/2}$ which is however broken and replaced by $P_x = e^{i\pi a^\dagger a}$ in the full quadratic form here. The bias is also an asymmetric term but there is a hidden symmetry at certain points in linear-coupling situation [86–88]. The coupling mixing breaks all the symmetries and leads to rich QPTs [36].

By transformation $a^\dagger = (\hat{x} - i\hat{p})/\sqrt{2}$, $a = (\hat{x} + i\hat{p})/\sqrt{2}$ with position x and momentum $\hat{p} = -i\frac{\partial}{\partial x}$, we can rewrite H as [30, 35, 36, 89] $H_x = \sum_{\sigma_z=\pm} h_{\sigma_z} |\sigma_z\rangle \langle \sigma_z| + \frac{\Omega}{2} \sum_{\sigma_z=\pm} |\sigma_z\rangle \langle \sigma_z|$ where $\sigma_z = -\bar{\sigma}_z = \pm$ labels the spin in z direction. Here $h_\pm = \frac{\omega}{2} \hat{p}^2 + v_\pm(x)$ is the effective single-particle Hamiltonian, in the spin-dependent harmonic potential

$$v_\pm(x) = \frac{\omega}{2} \varpi_\pm^2 (x \pm b_\pm)^2 + d_\pm(x) \mp \epsilon - \frac{\omega}{2}, \quad (2)$$

with frequency renormalization ϖ_\pm , displacement of potential bottom b_\pm , coupling-mixing-induced asymmetry d_\pm ,

$$\varpi_\pm = \sqrt{1 \pm g_2/g_T}, \quad (3)$$

$$b_\pm = \frac{g'_1}{1 \pm g_2/g_T}, \quad (4)$$

$$d_\pm = -\frac{\bar{g}_1^2 \Omega}{4(1 \pm \bar{g}_2)}, \quad (5)$$

and single-particle energy

$$\epsilon_\pm^0 = \omega(n + \frac{1}{2}) \sqrt{1 \pm \bar{g}_2} \mp \epsilon - \frac{1}{2} \omega. \quad (6)$$

In such a formalism the Ω term plays the role of spin flipping in the spin space or tunneling in the position space [30, 78, 89]. Hereafter we consider the ground state which involves $n = 0$.

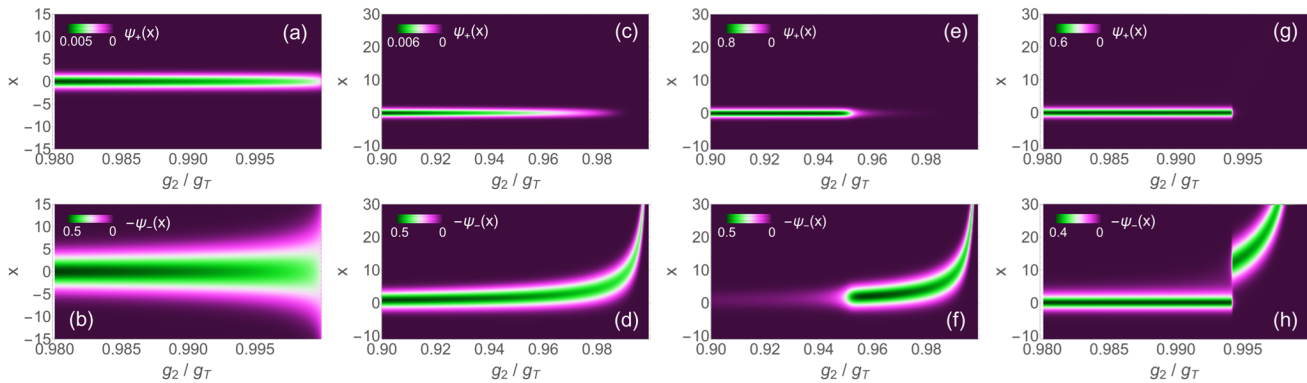


FIG. 1. Variation patterns of wave function and different sensitivity resources of quantum metrology. Wave function components ψ_+ (a,c,e,g) and ψ_- (b,d,f,h) with different parameters: (a) $\epsilon = 0$, $g_1 = 0$, $\Omega = 0.01\omega$, with squeezing resource. (b) $\epsilon = 0$, $g_1 = 1.2\omega$, $\Omega = 0.01\omega$, with squeezing and displacement resources. (c) $\epsilon = 0.33\omega$, $g_1 = 1.2\omega$, $\Omega = 0.01\omega$, with squeezing, displacement and transition resources. (d) $\epsilon = 0.33\omega$, $g_1 = 0.1\omega$, $\Omega = 1.0\omega$, with squeezing, displacement and transition resources at finite Ω . Here $\omega = 1$ is set for the unit. There is a degeneracy-lifting pattern around $g_2 = 0$ at $\epsilon = 0$ and $g_1 = 0$, with ψ_{\pm} varying similar to (e) and (f) after the transition point except the absence of displacement.

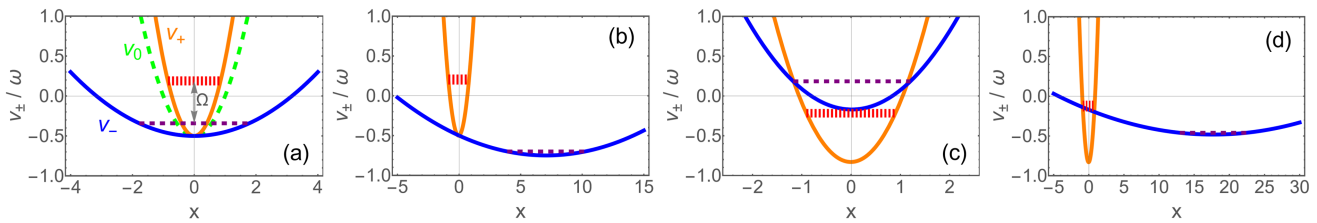


FIG. 2. Effective potential v_{\pm} and physical picture for the squeezing (a), displacement (b) and transition (c,d). (a) Narrowing of v_+ (orange solid) and broadening of v_- (blue solid) compared with the original potential v_0 (green long-dashed) at $g_2 = 0.9g_T$ with $g_1 = 0$ and $\epsilon = 0$. The horizontal red dotted line and purple dashed line represent ϵ_+ and ϵ_- , while the arrows indicate the spin flipping Ω . (b) Displaced v_- at $g_1 = 1.0g_s$ with $g_2 = 0.9g_T$ and $\epsilon = 0$. (c) Energy situation $\epsilon_- > \epsilon_+$ before the transition, at a finite bias $\epsilon = 0.33\omega$ with $g_1 = 0.1g_s$ and $g_2 = 0.5g_T$. (d) Reversed energy situation $\epsilon_- < \epsilon_+$ after the transition, at $g_2 = 0.998g_T$ with $\epsilon = 0.33\omega$ and $g_1 = 0.1g_s$. Here, $\Omega = 0.01\omega$ in all panels and we set $\omega = 1$ as the unit.

III. QUANTUM FISHER INFORMATION (QFI) FOR QUANTUM METROLOGY

In QM the measurement precision of experimental estimation on a parameter λ is bounded by $F_Q^{1/2}$ [90], where F_Q is the QFI defined as [90–92]

$$F_Q(\lambda) = 4 \left[\langle \psi'(\lambda) | \psi'(\lambda) \rangle - |\langle \psi'(\lambda) | \psi(\lambda) \rangle|^2 \right] \quad (7)$$

for a pure states $|\psi(\lambda)\rangle$. Here $'$ denotes the derivative with respect to the parameter λ . A higher QFI would mean a higher measurement precision. For a real wave function $\psi(\lambda)$, as is usually the case in non-degenerate states of a real Hamiltonian, the QFI can be simplified to be [43]

$$F_Q = 4 \langle \psi'(\lambda) | \psi'(\lambda) \rangle, \quad (8)$$

which also applies for the ground state of our Hamiltonian (1) considered in the present work.

It is worth mentioning that the appearance of the QFI peak not only can be employed for critical QM [1, 4–6]

but also signals a QFT in fidelity theory [93–97], as applied to identify the frequency dependence of the QPT in the quantum Rabi model [43]. In fact, in an infinitesimal parameter variation $\delta\lambda$ the fidelity F can be expand as

$$F = |\langle \psi(\lambda) | \psi(\lambda + \delta\lambda) \rangle| = 1 - \frac{\delta\lambda^2}{2} \chi_F, \quad (9)$$

thus the QFI is also the susceptibility of the fidelity by the correspondence $\chi_F = F_Q/4$ [94–96]. In our resources-combined QM addressed in the present work we will see peaks of QFI which are really coming from the transition resource.

IV. DIFFERENT VARIATION PATTERNS OF WAVE FUNCTION

From the QFI (7) one sees that the measurement precision comes from the sensitivity of the wave function change in response to the parameter variation. A quicker change of the wave function driven by the parameter variation means a larger QFI and a higher MP upper bound.

The mixed linear and nonlinear interactions in H provide various variation patterns of the wave function for the sensitivity resource.

The first pattern is the squeezing of the wave function. As illustrated in Figs. 1(a) and 1(b), with the variation of g_2 in approaching to g_T the wave-function component $\psi_+(x)$ tends to be narrower [Fig. 1(a)] while $\psi_-(x)$ becomes more extended [Fig. 1(b)], the former being position squeezing while the latter corresponding to momentum squeezing [98]. Such squeezing effect arises from the nonlinear coupling which renormalizes the frequency by ϖ_{\pm} in the effective harmonic potential $v_{\pm}(x)$ in Eq. (2). Correspondingly $v_+(x)$ becomes narrower and $v_-(x)$ becomes broader relatively to the original potential $v_0 = \frac{\omega}{2}x^2$, as demonstrated by Fig. 2(a). Note that the squeezing effect in $v_-(x)$ is divergently strong as $\varpi_- = \sqrt{1 - g_2/g_T}$ tends to vanish in the variation of g_2 when it approaches to g_T . Such a diverging behavior provides a resource of high sensitivity for QM.

The second pattern is the displacement of the wave packet. As illustrated in Fig. 1(d), the wave packet of $\psi_-(x)$ is moving quickly away from the origin ($x = 0$) when g_2 increases despite that the moving of $\psi_-(x)$ in the opposite direction is slower and less visible, as driven by the potential displacement b_{\pm} in the presence of a finite linear coupling illustrated in Fig. 2(b). Indeed, the moving acceleration of $\psi_-(x)$ becomes extremely large in the vicinity of g_T as $b_- = g'_1/(1 - g_2/g_T)$ is diverging. Such a diverging acceleration offers another resource of high sensitivity for QM.

The third pattern is the transition. In the presence of the bias, as shown in Fig. 2(c), the energy level ε_- (dotted line) can be higher than ε_+ (dashed line) for a small g_2 . An energy level reversal can occur when g_2 is enhanced, as one finds in Fig. 2(d), such an energy reversal induces a transition. Corresponding the density weight is also transiting quickly from $\psi_+(x)$ to $\psi_-(x)$, as displayed in Figs. 1(e) and 1(f). Such a transition supplies a third resource of high sensitivity for QM.

Finally there is also a degeneracy-lifting pattern arising at the symmetry breaking point. In fact, in the absence of the linear coupling, nonlinear coupling and bias field, the uncoupled and unbiased system has both spin-rotation symmetry $P_{\sigma} = \sigma x$ and U(1) symmetry $U(1) = e^{i\theta a^{\dagger}a}$ with an arbitrary phase θ . At such a highly symmetric point the two spin energy levels at any n are degenerate. Turning on the coupling e.g. the nonlinear one here, both the two symmetries are broken and the symmetry is lowered to be P_x with a limited phase $\theta = \pi$. As a consequence the level degeneracy is lifted. The behavior of the wave-function variation is similar to that after the transition in Fig. 2(c), with a variation from equal density weights on the two spin components at the degenerate point to unbalanced weights at a finite g_2 .

In the above analysis we see that the diverging origin in the squeezing pattern and the displacement pattern lies in the $\psi_-(x)$ component. For this reason, in the following we will first address the small- Ω regime, as illustrated

in Figs. 1(a)-1(f), which maximizes the contribution of $\psi_-(x)$, before showing the validity of these resources in the finite- Ω regime.

V. APPLICATIONS FOR QUANTUM METROLOGY

A. Quantum metrology by squeezing resource

Squeezing is a primary quantum resource that has been applied in quantum metrology[21–25]. As described in the first pattern of the wave function in last section, here in the nonlinear coupling of light-matter interaction the model (1) also manifests a squeezing effect which is divergently strong as a sensitivity resource for QM. We can see the pure squeezing effect at $\epsilon = 0$ and $g_1 = 0$. In this case, there is no displacement or transposition and in the small- Ω regime the ground-state wave function can be well approximated by $\psi_{\pm}(x) = c_{\pm}\varphi_{\pm}(x)$, where $\varphi_{\pm}(x) = \xi_{\pm}^{1/4} \exp[-\frac{1}{2}\xi_{\pm}x^2]/\pi^{1/4}$ is the ground state of quantum harmonic oscillator with renormalized frequency $\xi_{\pm} \cong \varpi_{\pm}$. In such a situation the QFI for the parameter g_2 contains two parts

$$F_Q(g_2) = F_Q^{\xi}(g_2) + F_Q^{\rho}(g_2), \quad (10)$$

respectively coming from the squeezing of the basis $\varphi_{\pm}(x)$ and the variation of spin-component density or weight (see the derivation in Appendix B).

$$F_Q^{\xi}(g_2) = \left[\frac{c_+^2}{8(1+\bar{g}_2)^2} + \frac{c_-^2}{8(1-\bar{g}_2)^2} \right] \frac{1}{g_T^2}, \quad (11)$$

$$F_Q^{\rho}(g_2) = \frac{(\bar{g}_2 dw + 8w_2 \bar{w}^3)^2 S_{\Omega}^2 \omega^2}{4w_2^4 (16S_{\Omega}^2 + dw^2 \omega^2)^2 \bar{w}^4 g_T^2}, \quad (12)$$

where

$$S_{\Omega}^2 = \left(\frac{\Omega}{2} \langle \varphi_+ | \varphi_- \rangle \right)^2 = w_2^{1/2} \Omega^2 / (4\bar{w}), \quad (13)$$

$$c_+^2 = \frac{\frac{1}{2} \left(\sqrt{\omega^2 dw^2 + 16S_{\Omega}^2} - \omega dw \right)^2}{16S_{\Omega}^2 + \omega^2 dw^2 - \omega dw \sqrt{\omega^2 dw^2 + 16S_{\Omega}^2}}, \quad (14)$$

$$c_-^2 = \frac{8S_{\Omega}^2}{16S_{\Omega}^2 + \omega^2 dw^2 - \omega dw \sqrt{\omega^2 dw^2 + 16S_{\Omega}^2}}, \quad (15)$$

and we have defined $\bar{w} = (\varpi_+ + \varpi_-)/2$, $dw = (\varpi_+ - \varpi_-)$, $w_2 = \varpi_+ \varpi_-$ and $\varpi_{\pm} = \sqrt{1 \pm \bar{g}_2}$.

1. Criticality of QFI

In approaching $\bar{g}_2 = 1$ both $F_Q^{\xi}(g_2)$ and $F_Q^{\rho}(g_2)$ are diverging in a critical way

$$F_Q^{\xi}(\bar{g}_2) \sim \frac{1}{(1-\bar{g}_2)^2} \frac{1}{\omega^2}, \quad (16)$$

$$F_Q^{\rho}(g_2) \sim \frac{1}{(1-\bar{g}_2)^{7/4}} \frac{\Omega^2}{\omega^4}, \quad (17)$$

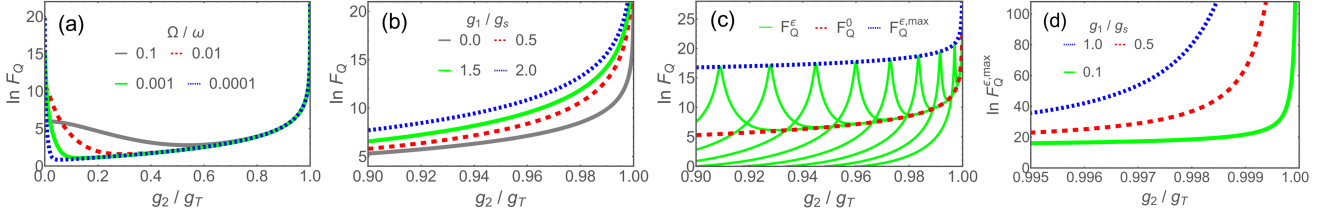


FIG. 3. The quantum Fisher information (QFI) F_Q (plotted in natural logarithm) in the presence of different resources. (a) $g_1 = 0$ and $\epsilon = 0$ at different frequency ratio $\Omega/\omega = 0.0001, 0.001, 0.01, 0.1$ with squeezing resource at finite g_2 and degeneracy-lifting resource around $g_2 = 0$. (b) $\epsilon = 0$ and $\Omega = 0.01\omega$ at different linear couplings $g_1/g_s = 0.0, 0.5, 1.5, 2.0$ with squeezing and displacement resources. (c) the QFI F_Q^ϵ by different $\epsilon/\omega = 0.27 \sim 0.34$ [green (light gray) solid] in spacing 0.01 at $g_1 = 0.1g_s$ and $\Omega = 0.001\omega$, with squeezing, displacement and transition resources. The red dashed line denotes the QFI F_Q^0 without transition resource ($\epsilon = 0$), while the blue dotted line provides the peak value $F_Q^{\epsilon,max}$ continuously yielded by tuning ϵ . (d) $F_Q^{\epsilon,max}$ at different linear couplings $g_1/g_s = 0.1, 0.5, 1.0$ at $\Omega = 0.01\omega$. In all panels, $\omega = 1$ is set to be the unit.

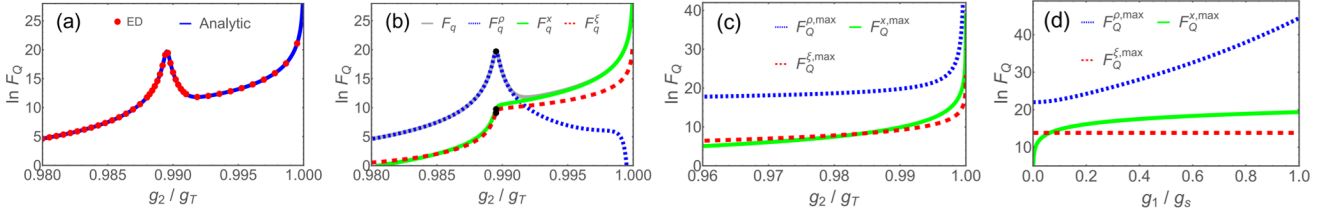


FIG. 4. Tracking the contributions of different sensitivity sources. (a) Comparison of total F_q for the analytic result (blue solid line) and the exact diagonalization (ED) result (red dots). (b) Contributions of F_Q^ξ (red dashed), F_Q^x (green solid) and F_Q^ρ (blue dotted) in total F_Q (gray solid). The black dots in (b) mark the analytic $F_Q^{\xi,max}$, $F_Q^{x,max}$ and $F_Q^{\rho,max}$ at the transition point in Eqs. (??). Here $\epsilon = 0.33\omega$ and $g_1 = 0.5g_s$. (c) Evolution of $F_Q^{\xi,max}$, $F_Q^{x,max}$ and $F_Q^{\rho,max}$ versus g_2 at fixed $g_1 = 0.5g_s$. (d) Evolution of $F_Q^{\xi,max}$, $F_Q^{x,max}$ and $F_Q^{\rho,max}$ versus g_1 at fixed $g_2 = 0.999g_T$. We set $\Omega = 0.001\omega$ and the unit $\omega = 1$ in all panels.

The critical exponents, defined by $F_Q^i(g_2) \sim (1 - \bar{g}_2)^{-\gamma_i}$, are

$$\gamma_\xi = 2, \quad \gamma_\rho = 7/4, \quad (18)$$

respectively. As afore-mentioned, the critical behavior of $F_Q^\xi(\bar{g}_2)$ is the result of the basis variation with vanishing frequency ϖ_- which leads to a divergently strong momentum squeezing. The diverging behavior of $F_Q^\rho(g_2)$ arises from the w_+^4 factor, partially canceled by $w_+^{1/2}$ in S_Ω^2 , which is the result of the variation speed of the wavepacket overlap $S_\Omega = \frac{\Omega}{2} \langle \varphi_+ | \varphi_- \rangle$ and also originates from the squeezing effect. Thus, here we have a high sensitivity resource for QM purely from squeezing.

2. Universality of QFI

It should be noted that $F_Q^\xi(\bar{g}_2)$ is more dominant than $F_Q^\rho(g_2)$ in the above case. Although the magnitudes of the critical components γ_ξ in $F_Q^\xi(\bar{g}_2)$ and γ_ρ in $F_Q^\rho(g_2)$ are comparable, the contribution of $F_Q^\rho(g_2)$ is diminished by the Ω^2 factor in the small- Ω regime. Physically, in the increase of \bar{g}_2 , the system becomes nearly fully polarized due to the splitting frequencies ϖ_\pm and the weak spin flipping strength Ω . Consequently, the final diverging

behavior of the total QFI $F_Q(g_2)$ in the vicinity of $\bar{g}_2 = 1$ is dominated by the singular behavior of $F_Q^\xi(\bar{g}_2)$ which is little affected by Ω . This accounts for the universality of $\ln F_Q(g_2)$ in different Ω values, as we see in Fig.3(a) in the regime $\bar{g}_2 \in [0.6, 1]$.

It is worthy to mentioned that the criticality and universality of QFI were noticed around the exceptional points in non-Hermitian Jaynes-Cummings Models [11] as another fundamental model of light-matter interaction. Here we have the Hermitian situation. The criticality of QFI promises a divergently high measurement precision, while the universality of QFI guarantees a same high order of measurement precision for different tunneling or spin flipping strengths.

B. Quantum metrology by degeneracy lifting

In Fig.3(a) we also see a diverging-like behavior of the QFI in small- \bar{g}_2 regime for small Ω values. Such a diverging-like behavior comes from $F_Q^\rho(g_2)$, via the key factor $F_Q^\rho(g_2) \sim \left(16 \frac{S_\Omega}{\omega} + dw^2 \frac{\omega}{S_\Omega}\right)^{-2} \frac{1}{g_T^2}$, which is varying in a singular-like manner

$$F_Q^\rho(g_2) \sim \frac{1}{g_2^4 g_T^2}, \quad \text{for } \Omega^2 \ll \bar{g}_2^2 \omega^2, \quad (19)$$

with respect to \bar{g}_2 and a maximum value

$$F_Q^\rho(g_2) = \frac{\omega^2}{4\Omega^2} \frac{1}{g_T^2}, \quad \text{at } \bar{g}_2 = 0, \quad (20)$$

diverging with respect to the small- Ω limit.

In fact, these behaviors come from the degeneracy lifting in symmetry breaking mentioned in Sec. IV, as the energies in the opposite spin are degenerate at $\bar{g}_2 = 0$ while the degeneracy is lifted once a finite \bar{g}_2 is turned on. The density weights of the two spin components become unbalanced quickly under a weak spin flipping strength Ω . This fast weight variation provides a sensitivity resource in the small- \bar{g}_2 regime. It should be mentioned that, although the squeezing vanishes right at $\bar{g}_2 = 0$, there is still a finite contribution from the squeezing resource

$$F_Q^\xi(g_2) = \frac{1}{8g_T^2}, \quad \text{at } \bar{g}_2 = 0. \quad (21)$$

This finite contribution remains due to the fact that the QFI depends on the response to the parameter variation, rather than the parameter at one point, while the derivative with respect to \bar{g}_2 is not vanishing even at $\bar{g}_2 = 0$.

Since generally in QM squeezing is a more-applied resource, in the following we shall focus more on the regime in the vicinity of $\bar{g}_2 = 1$ where the squeezing strength becomes divergently strong.

C. Quantum metrology by combining squeezing and displacement resources

When the linear coupling g_1 is also turned on, we get another resource from displacement which can be combined with the squeezing resource. The linear coupling gives rise to a displacement b_\pm with opposite directions in the two spin components, as in Eq. (4). Indeed, in the situation of $g_1 \neq 0$ and $\epsilon = 0$, the displacement adds the contribution F_Q^x to the total QFI

$$F_Q(g_2) = F_Q^\xi(g_2) + F_Q^\rho(g_2) + F_Q^x(g_2). \quad (22)$$

Here F_Q^ξ has the same form as in (11) except for the detail in the expressions of c_\pm^2 [see Eqs. (A5)-(A9)], while the displacement part reads (see the derivation in Appendix B)

$$F_Q^x(g_2) = \left[\frac{c_+^2}{(1+\bar{g}_2)^{7/2}} + \frac{c_-^2}{(1-\bar{g}_2)^{7/2}} \right] \frac{\bar{g}_1^2 \Omega}{\omega g_T^2}. \quad (23)$$

Note that the interplay of the linear and nonlinear couplings induces the additional potential difference $d_\pm(x)$ in (5) which enhances the spin polarization. In such a situation we can neglect the F_Q^ρ as there is little space left for the weight variation in almost full polarization due to the much-weakened tunneling between the displaced

wave packets. Thus, in the leading term, the total QFI has the form

$$F_Q(g_2) = \left[\frac{1}{8(1-\bar{g}_2)^2} + \frac{\bar{g}_1^2 \Omega / \omega}{(1-\bar{g}_2)^{7/2}} \right] \frac{1}{g_T^2} \quad (24)$$

as a result of the combined squeezing and displacement resources.

We see that the displacement resource yields a larger critical exponent γ_x than that of the squeezing resource,

$$\gamma_\xi = 2, \quad \gamma_x = 7/2, \quad (25)$$

unlike the smaller one $\gamma_\rho = 7/4$ in (18). On the other hand, the weakening factor Ω/ω of the displacement term in (24) is of lower order than Ω^2/ω^2 in (17). For these reasons F_Q^x can add a contribution even larger than F_Q^ξ despite the weakening factor Ω/ω in the small- Ω regime. In Fig.3(b) we see that the QFI is indeed enhanced by the presence of the linear coupling g_1 in comparison with the case in the absence of g_1 .

D. Quantum metrology by combining squeezing, displacement and transition resources

1. *Most divergent QFI by a broadest combination of the squeezing, displacement and transition resources*

Now we propose a broadest combination of the squeezing, displacement and transition resources. The squeezing has been produced by the nonlinear coupling g_2 and the displacement has been driven by the linear coupling g_1 as addressed in Sections VA and VC, while here the transition can be introduced by turning on a finite bias field ϵ , as analyzed in Sec. IV. In the presence of all finite values of the linear coupling g_1 , nonlinear coupling g_2 and bias field ϵ , the QFI can be also decomposed into three parts $F_Q = F_Q^\xi + F_Q^x + F_Q^\rho$. Around the transition a peak of QFI emerges, with the maximum value of the QFI also comprising of three contributions

$$F_Q^{\max}(g_2) = F_Q^{\xi, \max}(g_2) + F_Q^{x, \max}(g_2) + F_Q^{\rho, \max}(g_2) \quad (26)$$

respectively from the squeezing, displacement and transition resources. Since the transition occurs around the level crossing which has the equal spin-component weights, $c_+^2 = c_-^2 = 1/2$, we obtain

$$F_Q^{\xi, \max} = \frac{(1+\bar{g}_2^2)}{8(1-\bar{g}_2^2)^2 g_T^2}, \quad (27)$$

$$F_Q^{x, \max} = \left[\frac{1}{(1-\bar{g}_2)^{7/2}} + \frac{1}{(1+\bar{g}_2)^{7/2}} \right] \frac{\bar{g}_1^2 \Omega}{2\omega g_T^2}, \quad (28)$$

$$F_Q^{\rho, \max} = \frac{\bar{w} [w_2^3 \bar{w} \omega + \bar{g}_1^2 (1+\bar{g}_2^2) \Omega]^2}{4w_2^{17/2} \Omega^2 g_T^2} \exp\left[\frac{\bar{g}_1^2 \Omega}{w_2^3 \bar{w} \omega}\right] \quad (29)$$

Compared with the critical modes from the squeezing and displacement resources

$$F_Q^{\xi, \max}(g_2) \sim (1 - \bar{g}_2)^{-\gamma_\xi^{\max}}, \quad (30)$$

$$F_Q^{x, \max}(g_2) \sim (1 - \bar{g}_2)^{-\gamma_x^{\max}}, \quad (31)$$

with the critical exponents

$$\gamma_\xi^{\max} = 2, \quad \gamma_x^{\max} = 7/2, \quad (32)$$

the transition resource manifests a much more divergent trend compositely with a power divergence and an exponential divergence

$$F_Q^{\rho, \max} \sim (1 - \bar{g}_2)^{-\gamma_\rho^{\max}} \exp\left[\frac{\bar{g}_1^2 \Omega}{\bar{\omega} \omega \omega_+^3} (1 - \bar{g}_2)^{-\gamma_{\rho, \text{exp}}^{\max}}\right] \quad (33)$$

with the critical components

$$\gamma_\rho^{\max} = 17/4, \quad \gamma_{\rho, \text{exp}}^{\max} = 3. \quad (34)$$

In Fig.3(c), the green solid lines show the evolutions of $F_Q(g_2)$ in some continual values of the bias field ϵ under given finite values of g_2 and g_1 , each having a peak of QFI. A continuous tuning of the bias field yields the maximum QFI F_Q^{\max} (blue dotted line). One sees that the resource combination with the transition achieves several orders of improvement of the QFI over the uncombined case (red dashed line). Far more orders of improvements can be realized by further increasing of g_1 , as demonstrated in Fig.3(d).

2. Tracking the contributions of the difference resources

The results presented in Fig. 3(c) and 3(d) are the total QFI. To give a better view of the resource combination, we track the contributions of $F_Q^\xi(g_2)$, $F_Q^\rho(g_2)$, and $F_Q^x(g_2)$ separately in Fig. 4. To confirm the analytic analysis in the above we first compare in Fig. 4(a) the analytic result (blue solid) and the exact diagonalization result (ED, red dots) of F_Q , which shows a complete agreement. The full analytic expressions for F_Q^ξ , F_Q^x , F_Q^ρ , and F_Q are obtained in Appendix B, while a brief description of the ED method for QFI [35, 36, 43] is presented in Appendix D. The separate contributions of the three resources to the QFI are plotted in Fig. 4(b). This contribution tracking shows the divergent tendency of F_Q^ξ (red dashed) and F_Q^x (green solid), while the peak profile in the total QFI F_Q (gray solid) really comes from the transition resource in F_Q^ρ (blue dotted). The black dots at the peak position mark the analytic values of $F_Q^{\xi, \max}$, $F_Q^{x, \max}$, and $F_Q^{\rho, \max}$ which match the results of F_Q^ξ , F_Q^x , and F_Q^ρ . The evolutions of $F_Q^{\xi, \max}$, $F_Q^{x, \max}$, and $F_Q^{\rho, \max}$ are displayed in Fig. 4(c), which shows the differences in their divergence strengths, with achievable higher orders of $F_Q^{\rho, \max}$ over the competing $F_Q^{\xi, \max}$ and $F_Q^{x, \max}$. The order differences can be tuned by g_1 as shown in Fig. 4(d).

3. Comparison with combination of the squeezing and transition resources.

In the previous sections we have added and combined the sensitivity resources step by step from squeezing, displacement, and transition. There is a combination missing between the squeezing and transition resources which may be worthy to compare. Setting $\bar{g}_1 = 0$ gives the result of such combination of the squeezing and transition resources without the displacement

$$F_Q^{\xi, \max}(g_2) = \frac{(1 + \bar{g}_2^2)}{8(1 - \bar{g}_2^2)^2 g_T^2}, \quad (35)$$

$$F_Q^{\rho, \max}(g_2) = \frac{\bar{\omega}^3 \omega^2}{4(1 - \bar{g}_2^2)^{5/4} \Omega^2} \frac{1}{g_T^2}. \quad (36)$$

Despite that the critical exponent γ_ρ^{\max} from the transition resource is smaller than that from the squeezing resource, as

$$\gamma_\rho^{\max} = 5/4, \quad \gamma_{\rho, \text{exp}}^{\max} = 2, \quad (37)$$

here in (35) and (36), $F_Q^{\rho, \max}(g_2)$ is greatly amplified by the enhancing factor ω^2/Ω^2 with a strong divergence with respect to the small- Ω limit. Still, compared with the result in (33), we see that the broadest combination with the displacement resource provides a strongest boost for the enhancement of the QFI.

VI. MORE ADVANTAGES IN THE QUANTUM METROLOGY

Besides the upgrading of upper bound of measurement precision, the protocol of resource combination also has several other advantages including more global parameter regime, breaking the frequency-limit restriction, and finite preparation time of probe state (PTPS), as addressed in the following.

A. Global parameter regime

It should be mentioned that the transition resource is more flexible for tuning. Actually the transition may be tuned to any position by the bias and the linear coupling. Indeed, the transition can be manipulated to occur at a wanted value of \bar{g}_2 by adding the bias $\epsilon = \epsilon_{\max}$ under a given \bar{g}_2 or the linear coupling $\bar{g}_1 = \bar{g}_1^{\max}$ under a given ϵ :

$$\epsilon_{\max} = \frac{\omega}{4} (\sqrt{1 + \bar{g}_2} - \sqrt{1 - \bar{g}_2}) + \frac{\bar{g}_1^2 \bar{g}_2 \Omega}{4(1 - \bar{g}_2^2)}, \quad (38)$$

$$\bar{g}_1^{\max} = \sqrt{\frac{4(1 - \bar{g}_2^2)}{\bar{g}_2 \Omega} \left[\epsilon - \frac{\omega}{4} (\sqrt{1 + \bar{g}_2} - \sqrt{1 - \bar{g}_2}) \right]} \quad (39)$$

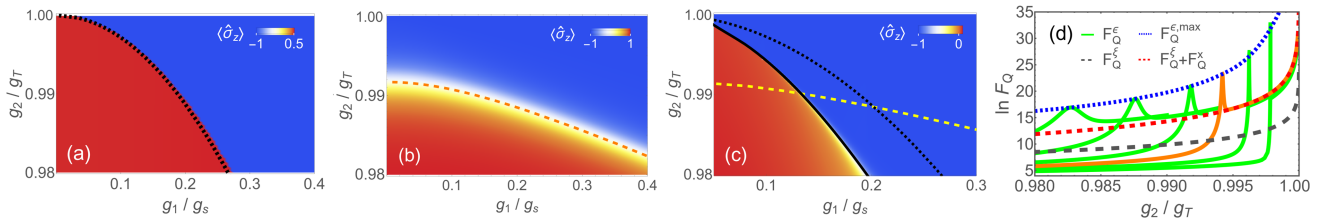


FIG. 5. Breaking the frequency limitation. (a-c) Phase diagram of $\langle \hat{\sigma}_z \rangle$ in the g_1 - g_2 plane at $\omega/\Omega = 0.01$ (a), $\Omega/\omega = 0.01$ (b), and $\omega/\Omega = 1.0$ (c). (d) Maximum QFI $F_Q^{\epsilon, max}$ over F_Q^ϵ (green solid) in varying g_1 at $\omega/\Omega = 1.0$. In (d) the example of F_Q^ϵ at $g_1 = 0.1g_s$ (orange solid) is compared with $F_Q^\epsilon + F_Q^x$ (red dashed) and F_Q^ϵ (gray long-dashed). In all panels $\epsilon = 0.33$ and $\max\{\omega, \Omega\} = 1$ is set to be the unit.

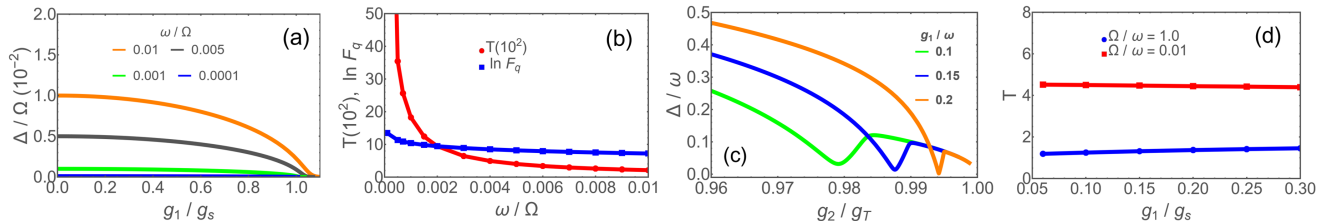


FIG. 6. Reduction of the preparation time of the probe state (PTPS). (a) Gap Δ in linear interaction at low frequencies. (b) Gap F_Q (blue squares) and PTPS T in unit of 10^2 (red dots) in linear interaction at low frequencies. (c) Gap Δ in linear interaction in the presence of different g_1 at $\Omega/\omega = 1$. (d) T (in unit of 1) versus g_1 at $\Omega/\omega = 1$ (blue dots) and $\Omega/\omega = 0.01$ (red squares).

Setting $\epsilon_{\max} = 0$ and $\bar{g}_1^{\max} = 0$ will retrieve and connect the case of the degeneracy-lifting resource discussed in Sec. VB, thus covering the entire parameter range of \bar{g}_2 .

This degree of freedom in tuning allows a more global validity regime and flexibility for manipulation of QM, in contrast to the linear critical QM in which the transition only occurs at a single coupling point.

B. Breaking the frequency-limit restriction

The favorable condition for the linear critical QM is the low-frequency limit $\omega/\Omega \rightarrow 0$, while at finite frequencies the QFI becomes much diminished [6, 43]. Such a frequency-limit restriction is however broken in the protocol proposed in the present work. Indeed, we have the transition resource in all frequency regimes. Actually the transition resource is available both in the small- Ω regime and in the low-frequency regime, as shown by the phase diagrams of $\langle \hat{\sigma}_z \rangle$ in Figs. 5(a) and 5(b). The transition boundary in the small- Ω regime has been given in (38) and (39), while the transition boundary in the low-frequency limit is provided by [36]

$$\bar{g}_{1c} = \left(1 + \frac{1}{\bar{g}_2} \frac{\epsilon}{\Omega}\right) \sqrt{1 - \bar{g}_2^2}, \quad (40)$$

as denoted by the dotted line and dashed line in Figs. 5(a) and 5(b). It is particularly worth noting that the transition resource also remains in the finite Ω and finite ω regime, as demonstrated by the phase diagram of $\langle \hat{\sigma}_z \rangle$ in Fig. 5(c). In fact, all resources of squeezing, displacement

and transitions survive in the finite Ω and finite ω regime, as demonstrated by the wave function in Figs. 1(g) and 1(h).

The QFI in the finite Ω and finite ω regime is illustrated in Fig. 5(d), with the divergence behavior and resource contributions similar to Fig. 3(c) in the small- Ω regime. Here, a bit differently for the plots, the large- \bar{g}_2 tails of $F_Q(g_2)$ in Fig. 5(d) do not collapse into the same line as in Fig. 3(c), due to that we illustrate by tuning g_1 at a fixed ϵ in the former rather than ϵ at fixed g_1 the latter. This difference can be seen from $F_Q^x(g_2)$ of the displacement resource in (23) and (24) which depends on g_1 but is little affected by ϵ .

In particular, in Fig. 5(d) we give a comparison for the analytic result (24) of $F_Q^\epsilon + F_Q^x$ (red dashed) without transition at $\epsilon = 0$ and the ED result of F_Q (orange solid) with transition at the finite ϵ . We see that they agree well with each other after the transition, which not only confirms the analytic result by ED but also indicates that the physical picture of resource combination in the small- Ω regime also applies for the finite- Ω regime. On the other hand, the peak position of $F_Q(g_2)$ by continuously varying g_1 in Fig. 5(d) is marked as the black solid line in Fig. 5(c), which matches well with the transition boundary of $\langle \hat{\sigma}_z \rangle$ there, indicating that the peak contribution also really comes from the transition just like in the small- Ω regime. With these confirmations, a comparing for the long-dashed line (F_Q^ϵ with only squeezing resource), the red dashed line ($F_Q^\epsilon + F_Q^x$ by combined squeezing and displacement resources), and the blue dotted line ($F_Q^{\epsilon, max}$ by

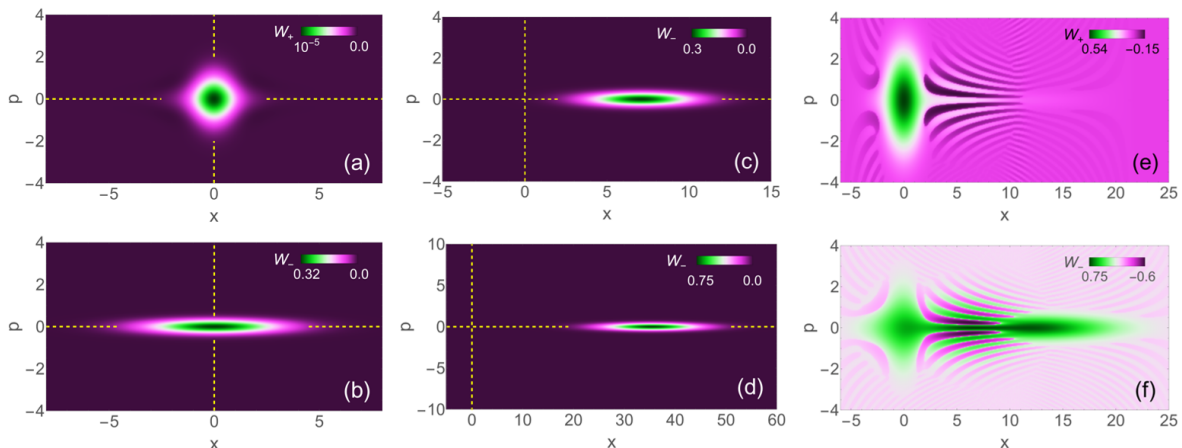


FIG. 7. The Wigner function $W_\sigma(x, p)$ in the presence of different resources. Squeezing resource: (a,b) $g_1 = 0$, $\epsilon = 0$, $g_2 = 0.99g_T$ and $\Omega = 0.01\omega$ for $\sigma = +$ (a) and $\sigma = -$ (b). Squeezing and displacement resources: (c) $\sigma = -$, $g_1 = 1.0g_s$, $\epsilon = 0$, $g_2 = 0.998g_T$ and $\Omega = 0.01\omega$. Squeezing, displacement and transition resources: (d) after transition, $\sigma = -$, $g_1 = 1.0g_s$, $\epsilon = 0.33\omega$, $g_2 = 0.998g_T$ and $\Omega = 1.0\omega$. (e,f) around transition, $\sigma = +$, $g_1 = 0$, $\epsilon = 0$, $g_2 = 0.9942g_T$ and $\Omega = 1.0\omega$ for $\sigma = +$ (e) and $\sigma = -$ (f). The crossing of the dashed lines in (a-d) marks the origin. In all panels, $\omega = 1$ is set to be the unit. In (e,f) the plotted amplitude is amplified by $|W_\sigma|^{1/4}$.

combined all three resources of squeezing, displacement and transition) demonstrates the upgrading by resource combinations also in the finite- Ω regime.

More exactly speaking, in the finite Ω and finite ω regime, the combined resources are more entangled and, unlike in the small- Ω regime, the mixed terms $F_Q^{\xi,x}$, $F_Q^{\xi,\rho}$, and $F_Q^{x,\rho}$ in the QFI do not completely vanish:

$$F_Q = F_Q^\xi + F_Q^x + F_Q^\rho + F_Q^{\xi,x} + F_Q^{\xi,\rho} + F_Q^{x,\rho}, \quad (41)$$

due to the emergence of anti-polaron wave packets[30]. Nevertheless, as the intra-polaron terms in F_Q^ξ , F_Q^x , and F_Q^ρ are still playing a leading role, we also have a diverging QFI from the different sensitivity resources qualitatively similar to the small- Ω regime, as addressed in the above for Fig 5(d). We leave the expressions and corresponding discussion in Appendix C.

C. Finite gap and preparation time of probe state (PTPS)

Another detrimental problem in the linear critical QM is the divergent PTPS. The PTPS is inversely proportional to the gap Δ in adiabatic preparation of the probe states, so that the PTPS can be estimated by [1, 6]

$$T = \int_0^{\bar{g}_{\max}} \Delta(\bar{g})^{-1} d\bar{g} \quad (42)$$

where $\bar{g} = \bar{g}_1$ for the linear critical QM ($\bar{g} = \bar{g}_2$ for the nonlinear coupling in the present work) and \bar{g}_{\max} is the rescaled transition point where the QFI has a peak

value [43]. In linear coupling, the gap tends to over-all close when the frequency is lowered as indicated in Fig. 6(a), consequently the PTPS T becomes diverging in the low-frequency limit as shown by the red dots in Fig. 6(b). In contrast, in the mixed nonlinear and linear couplings discussed in the present work, the gap (see Appendix A)

$$\Delta = 2\sqrt{e_-^2 + S_\Omega^2} \quad (43)$$

is finite either in the small- Ω regime or in the finite- Ω regime, as the order of gap is decided by ω [see (A10) in Appendix A] which is now not necessary to be in the low-frequency limit. We illustrate the finite gap in Fig. 6(c). As a result, the PTPS T is also finite, as in Fig. 6(d). Indeed, despite that the value of Ω is reduced by two orders, the PTPS is still in the same order of single digit, in a sharp contrast to the much larger order (unit of 10^2) and diverging behavior of the linear coupling case in Fig. 6(b). Thus, our present QM protocol also avoids the problem of diverging PTPS.

VII. WIGNER FUNCTION AND RESOURCES EXPLOITING FROM ALL THE POSITION, MOMENTUM, AND SPIN SPACES

We have seen that the combination of the squeezing, displacement and transition resources leads to a maximization of QFI and an upgrade of critical QM. As a more general view of point, actually the combination exploits the sensitivity resources from all the position, momentum, and spin spaces, which can be seen from the

Wigner function [99, 100]

$$W_{\pm}(x, p) = \frac{1}{2\pi} \int_{-\infty}^{\infty} e^{ipy} \psi_{\pm}^*(x + \frac{y}{2}) \psi_{\pm}(x - \frac{y}{2}) dy, \quad (44)$$

where we have set $\hbar = 1$. From $W_{\pm}(x, p)$ we can visualize all the distribution information of the position, momentum, and spin spaces. Figures 7(a) and 7(b) show $W_{\pm}(x, p)$ in a pure squeezing resource, we see a strong momentum squeezing in $W_{-}(x, p)$ along the p -axis direction despite that the position squeezing in $W_{+}(x, p)$ along the x -axis direction is not so obvious. Figure 7(b) includes both the presences of the squeezing and displacement resources, besides the momentum squeezing in $W_{-}(x, p)$ the wave packet distribution is shifting away from the origin (crossing point of the dotted lines). In this displaced case the momentum squeezing is termed as phase squeezing, while the position squeezing is called amplitude squeezing [98]. An example in the presence of transition resource is given in Figs. 7(e) and 7(f), the weight distributions of the main wave packets (red broad regions) are transferring from $W_{+}(x, p)$ to $W_{-}(x, p)$. On the other hand, we see that, besides the large displacement around $x = 15$ in $W_{-}(x, p)$, the amplitude and phase squeezings are still remaining. There are some fringes between and around the main wave packets, due to the interference of the two separating wavepackets, the visibility of which is actually amplified by plotting $|W_{\pm}(x, p)|^{1/4}$. Here Figures 7(a)-7(c) are illustrated for the small- Ω , while Figures 7(a)-7(c) show the example at a finite value of Ω . We see that the combination of squeezing, displacement and transition paves a way to exploit and combines resources for QM from all the position, momentum, and spin spaces.

VIII. CONCLUSIONS

We have proposed to combine various sensitivity resources to upgrade the upper bound of measurement precision in QM. Such protocol can be realized in light-matter-interaction system with mixed linear and non-linear couplings in the presence of bias field. Indeed, the system provides several quantum resources, including squeezing, degeneracy lifting, displacement and quantum phase transition, all with high sensitivity. We have analytically obtained the critical components or exponential behavior of QFI which represents the upper bound of measurement precision. We have combined and compared these resources step by step, each combination can give a dramatic boost to the enhancement of the QFI. Finally a broadest combination of squeezing, displacement and quantum phase transition yields a maximized QFI with an improvement by many orders over the widely-used squeezing resource.

In particular, in the broadest combination as aforementioned, the critical components for the diverging QFI

are $\gamma_{\xi}^{\max} = 2$ for the squeezing resource, $\gamma_x^{\max} = 7/2$ for the displacement resource, $\gamma_{\rho}^{\max} = 17/4$ for the transition resource, and the divergence from transition resource is even enhanced exponentially with an extra critical component $\gamma_{\rho, \text{exp}}^{\max} = 3$ inside the exponential factor. It is surprising to see here that the divergence of squeezing, which is the mostly exploited resource for QM, is relatively the least divergent resource, with the smallest critical component. Unexpectedly, the displacement resource can yield a stronger sensitivity and the transition resource is the strongest.

Besides the upgrading of the upper bound of measurement precision, our protocol of QM also exhibits several other advantages: (i) the parameter regime with high measurement precision is tunable and global, while the linear critical QM is locally limited to one critical point in our protocol; (ii) The frequency-limit restriction in the linear critical QM is broken; (iii) Our protocol avoids the detrimental problem of diverging PTPS which was also encountered in the linear critical QM.

Finally we have also analyzed the sensitivity resources via the Wigner function to gain a more general view. Indeed, our protocol exploits and combines all the resources in momentum, position and spin spaces to maximize the MP, while simultaneously the applicable regime is much more extended and condition restriction released.

ACKNOWLEDGMENT

This work was supported by the National Natural Science Foundation of China (Grants No. 12474358, No. 11974151, and No. 12247101).

Appendix A: Wave function and gap in small- Ω regime

In the small- Ω regime the ground-state wave function can be well approximated by $\psi_{\pm}(x) = c_{\pm}\varphi_{\pm}(x)$ where

$$\varphi_{\pm}(x) = \xi_{\pm}^{1/4} \exp[-\frac{1}{2}\xi_{\pm}(x \pm x_{\pm})^2]/\pi^{1/4} \quad (A1)$$

is the ground state of the quantum harmonic oscillator with renormalized frequency ξ_{\pm} and displacement x_{\pm} . On the basis of $\varphi_{\pm}(x)$ the Hamiltonian can be represented in matrix form

$$H = \begin{pmatrix} \tilde{\varepsilon}_{+} & S_{\Omega} \\ S_{\Omega} & \tilde{\varepsilon}_{-} \end{pmatrix} \quad (A2)$$

in the subspace of the lowest energies, with the single-particle energy in the diagonal terms

$$\begin{aligned} \tilde{\varepsilon}_{\pm} &= \frac{\xi_{\pm}\omega}{4} + (1 \pm \bar{g}_2) \left[1 + 2\xi_{\pm}(x_{\pm} - b_{\pm})^2 \right] \frac{\omega}{4\xi_{\pm}} \\ &\quad - \frac{\bar{g}_1^2\Omega}{4(1 \pm \bar{g}_2)} \mp \epsilon - \frac{\omega}{2} \end{aligned} \quad (A3)$$

and the tunneling or spin-flipping energy $S_\Omega = \frac{\Omega}{2} \langle \varphi_+ | \varphi_- \rangle$ in the non-diagonal terms, explicitly

$$S_\Omega = \frac{(\xi_+ \xi_-)^{1/4} \Omega}{\sqrt{2}(\xi_+ + \xi_-)^{1/2}} \exp\left[-\frac{(x_+ + x_-)^2 \xi_+ \xi_-}{2(\xi_+ + \xi_-)}\right]. \quad (\text{A4})$$

The eigen energy $E^\eta = e_+ + \eta \sqrt{e_-^2 + S_\Omega^2}$, where $e_\pm = (\tilde{\varepsilon}_+ \pm \tilde{\varepsilon}_-)/2$, has two branches labelled by $\eta = \pm$, while the ground state takes $\eta = -$ and

$$c_+ = B_+ / \sqrt{B_+^2 + B_-^2}, \quad c_- = B_- / \sqrt{B_+^2 + B_-^2} \quad (\text{A5})$$

$$B_+ = (e_- - \sqrt{e_-^2 + S_\Omega^2}), \quad B_- = S_\Omega, \quad (\text{A6})$$

subject to normalization condition $c_+^2 + c_-^2 = 1$.

The energy difference of the two energy branches is

$$\Delta = E^+ - E^- = 2\sqrt{e_-^2 + S_\Omega^2} \quad (\text{A7})$$

which will the gap when there is no level crossing in the lowest excited states.

In principle ξ_\pm and x_\pm are variationally determined by minimization of E^- . Here in the small- Ω regime the basis $\varphi_\pm(x)$ is little affected by the weak tunneling or spin flipping so that we can approximately set

$$\xi_\pm = \varpi_\pm, \quad x_\pm = b_\pm, \quad (\text{A8})$$

which means that the basis follows the potential adiabatically. The single-particle energy is then simplified to be

$$\tilde{\varepsilon}_\pm = \varepsilon_\pm = \frac{1}{2} \varpi_\pm \omega - \frac{\bar{g}_1^2 \Omega}{4(1 \pm \bar{g}_2)} \mp \epsilon - \frac{\omega}{2} \quad (\text{A9})$$

and the gap becomes

$$\Delta = \sqrt{(\omega dw + \frac{\bar{g}_1^2 \bar{g}_2 \Omega}{1 - \bar{g}_2} - \epsilon)^2 + \frac{w_2^{1/2} \Omega^2 / (16\bar{w})}{\exp(\frac{2\bar{g}_1^2 \Omega}{w_2^3 \sqrt{2\bar{w}\omega})}}} \quad (\text{A10})$$

where $\bar{w} = (\varpi_+ + \varpi_-)/2$, $dw = (\varpi_+ - \varpi_-)$, $w_2 = \varpi_+ \varpi_-$ and $\varpi_\pm = \sqrt{1 \pm \bar{g}_2}$.

Appendix B: QFI in small- Ω regime

From Section III we have the simplified QFI for a real wave function [43]

$$F_Q = 4 \langle \psi'(\lambda) | \psi'(\lambda) \rangle^2. \quad (\text{B1})$$

Since the wave function $\psi_\pm(x) = c_\pm \varphi_\pm(x)$ introduced in Appendix A depends on the frequency renormalization ξ_\pm , the displacement x_\pm and the spin component weight c_\pm , the derivative with respect to the parameter $\lambda = g_2$ includes three parts

$$\psi'_\pm(g_2) = c_\pm \frac{d\varphi_\pm}{d\xi_\pm} \frac{d\xi_\pm}{dg_2} + c_\pm \frac{d\varphi_\pm}{dx_\pm} \frac{dx_\pm}{dg_2} + \frac{dc_\pm}{dg_2} \varphi_\pm. \quad (\text{B2})$$

Correspondingly the QFI contains three contributions

$$F_Q = F_Q^\xi + F_Q^x + F_Q^\rho \quad (\text{B3})$$

with

$$F_Q^\xi = 4 \sum_{\sigma=\pm} c_\sigma^2 \langle \frac{d\varphi_\sigma}{d\xi_\sigma} | \frac{d\varphi_\sigma}{d\xi_\sigma} \rangle \left(\frac{d\xi_\sigma}{dg_2} \right)^2, \quad (\text{B4})$$

$$F_Q^x = 4 \sum_{\sigma=\pm} c_\sigma^2 \langle \frac{d\varphi_\sigma}{dx_\sigma} | \frac{d\varphi_\sigma}{dx_\sigma} \rangle \left(\frac{dx_\sigma}{dg_2} \right)^2, \quad (\text{B5})$$

$$F_Q^\rho = 4 \sum_{\sigma=\pm} \left(\frac{dc_\sigma}{dg_2} \right)^2 = 4 \frac{B'_+ B_- - B_+ B'_-}{(B_+^2 + B_-^2)^2}, \quad (\text{B6})$$

coming from the squeezing, displacement and spin weight variation respectively. Note here that the mixed terms are vanishing

$$F_Q^{\xi,x} = 8 \sum_{\sigma=\pm} c_\sigma^2 \langle \frac{d\varphi_\sigma}{d\xi_\sigma} | \frac{d\varphi_\sigma}{dx_\sigma} \rangle \frac{d\xi_\sigma}{dg_2} \frac{dx_\sigma}{dg_2} = 0, \quad (\text{B7})$$

$$F_Q^{\xi,\rho} = 8 \sum_{\sigma=\pm} c_\sigma \langle \frac{d\varphi_\sigma}{d\xi_\sigma} | \varphi_\sigma \rangle \frac{d\xi_\sigma}{dg_2} \frac{dc_\sigma}{dg_2} = 0, \quad (\text{B8})$$

$$F_Q^{x,\rho} = 8 \sum_{\sigma=\pm} c_\sigma \langle \frac{d\varphi_\sigma}{dx_\sigma} | \varphi_\sigma \rangle \frac{dx_\sigma}{dg_2} \frac{dc_\sigma}{dg_2} = 0, \quad (\text{B9})$$

as the normalization condition and $\frac{d\varphi_\sigma(x)}{d\xi_\sigma} \frac{d\varphi_\sigma(x)}{dx_\sigma}$ as a product of even and odd functions of $(x \pm x_\pm)$ lead to vanishing expectations $\langle \frac{d\varphi_\sigma}{d\xi_\sigma} | \varphi_\sigma \rangle = \langle \frac{d\varphi_\sigma}{dx_\sigma} | \varphi_\sigma(x) \rangle = \langle \frac{d\varphi_\sigma}{d\xi_\sigma} | \frac{d\varphi_\sigma}{dx_\sigma} \rangle = 0$.

In terms of small- Ω conditions (A8),

$$\langle \frac{d\varphi_\pm}{d\xi_\pm} | \frac{d\varphi_\pm}{d\xi_\pm} \rangle = \frac{1}{8\xi_\pm^2} = \frac{1}{8(1 \pm \bar{g}_2)}, \quad (\text{B10})$$

$$\langle \frac{d\varphi_\pm}{dx_\pm} | \frac{d\varphi_\pm}{dx_\pm} \rangle = \frac{\xi_\pm}{2} = \frac{\sqrt{(1 \pm \bar{g}_2)}}{2}, \quad (\text{B11})$$

$$\frac{d\xi_\pm}{dg_2} = \pm \frac{1}{2\sqrt{(1 \pm \bar{g}_2)}} \frac{1}{g_T}, \quad (\text{B12})$$

$$\frac{dx_\pm}{dg_2} = \mp \frac{\bar{g}_1 \sqrt{\Omega/\omega}}{\sqrt{2}(1 \pm \bar{g}_2)^2} \frac{1}{g_T}, \quad (\text{B13})$$

we find

$$F_Q^\xi = \left[\frac{c_+^2}{8(1 + \bar{g}_2)^2} + \frac{c_-^2}{8(1 - \bar{g}_2)^2} \right] \frac{1}{g_T^2}, \quad (\text{B14})$$

$$F_Q^x = \left[\frac{c_+^2}{(1 + \bar{g}_2)^{7/2}} + \frac{c_-^2}{(1 - \bar{g}_2)^{7/2}} \right] \frac{\bar{g}_1^2 \Omega}{\omega g_T^2}, \quad (\text{B15})$$

$$F_Q^\rho = 4 \frac{B'_+ B_- - B_+ B'_-}{(B_+^2 + B_-^2)^2}, \quad (\text{B16})$$

where

$$B'_+ = \frac{dB_+}{dg_2} = \left(e'_- - \frac{e_- e'_- + S_\Omega S'_\Omega}{\sqrt{e_-^2 + S_\Omega^2}} \right) \frac{1}{g_T^2}, \quad (\text{B17})$$

$$B'_- = \frac{dB_-}{dg_2} = S'_\Omega, \quad (\text{B18})$$

and

$$S_\Omega = \frac{w_2^{1/4} \Omega}{\sqrt{4\bar{w}}} \exp\left(-\frac{\bar{g}_1^2 \Omega}{w_2^3 \sqrt{2\bar{w}\omega}}\right), \quad (\text{B19})$$

$$S'_\Omega = -\left\{ \frac{\bar{g}_2}{8w_2^2 \bar{w}^2} + \frac{12\bar{g}_2 \bar{w} - (7\bar{g}_2^2 - 1) dw}{8w_2^6 \bar{w}^2 \omega / [\bar{g}_1^2 \Omega]} \right\} \frac{S_\Omega}{g_T} \quad (\text{B20})$$

$$e_- = \frac{dw}{4} \omega + \frac{\bar{g}_1^2 \bar{g}_2}{4w_2^2} \Omega - \epsilon, \quad (\text{B21})$$

$$e'_- = \frac{1}{4} \left[\frac{\bar{w}}{w_2} \omega + \frac{\bar{g}_1^2 (1 + \bar{g}_2^2) \Omega}{w_2^4} \right] \frac{1}{g_T}. \quad (\text{B22})$$

Here c_\pm is given in (A5) with substitution of (A8) and we have defined $\bar{w} = (\varpi_+ + \varpi_-)/2$, $dw = (\varpi_+ - \varpi_-)$, $w_2 = \varpi_+ \varpi_-$ and $\varpi_\pm = \sqrt{1 \pm \bar{g}_2}$.

Appendix C: QFI in finite- Ω regime

In the finite- Ω regime, the tunneling or spin-flipping becomes strong so that the wave function is composed of more than one wave packets ($n_p \geq 1$)

$$\psi_\pm(x) = \sum_{a=1}^{n_p} c_\pm^a \varphi_\pm^a(x) \quad (\text{C1})$$

where

$$\varphi_\pm^a(x) = (\xi_\pm^a)^{1/4} \exp[-\frac{1}{2} \xi_\pm^a (x \pm x_\pm^a)^2] / \pi^{1/4}. \quad (\text{C2})$$

The wave packets include polarons with the position $\mp x_\pm^a$ around the potential bottom $\mp b_\pm^a$ of the same spin component and anti-polarons with the position $\mp x_\pm^a$ around the potential bottom $\pm b_\mp^a$ of the opposite spin component. A simplest description without loss of accuracy can be $n_p = 2$, representing one polaron and one anti-polaron in each spin component[30].

The variation of the wave function now includes all polarons

$$\frac{d\psi_\pm}{dg_2} = \sum_a^{n_p} \left(c_\pm^a \frac{d\varphi_\pm^a}{d\xi_\pm^a} \frac{d\xi_\pm^a}{dg_2} + c_\pm^a \frac{d\varphi_\pm^a}{dx_\pm^a} \frac{dx_\pm^a}{dg_2} + \frac{dc_\pm^a}{dg_2} \varphi_\pm^a \right). \quad (\text{C3})$$

Unlike in the small- Ω regime, the mixed terms $F_Q^{\xi,x}$, $F_Q^{\xi,\rho}$, and $F_Q^{x,\rho}$ should be picked up in the QFI

$$F_Q = F_Q^\xi + F_Q^x + F_Q^\rho + F_Q^{\xi,x} + F_Q^{\xi,\rho} + F_Q^{x,\rho}. \quad (\text{C4})$$

The pure-resource terms now include intra-polaron terms ($a = a'$) and inter-polaron terms ($a \neq a'$)

$$F_Q^\xi = \sum_a^{n_p} \sum_{a'}^{n_p} \sum_{\sigma=\pm} c_\sigma^a c_{\sigma'}^{a'} \left\langle \frac{d\varphi_\sigma^a}{d\xi_\sigma^a} \middle| \frac{d\varphi_{\sigma'}^{a'}}{d\xi_{\sigma'}^{a'}} \right\rangle \frac{d\xi_\sigma^a}{dg_2} \frac{d\xi_{\sigma'}^{a'}}{dg_2}, \quad (\text{C5})$$

$$F_Q^x = \sum_a^{n_p} \sum_{a'}^{n_p} \sum_{\sigma=\pm} c_\sigma^a c_{\sigma'}^{a'} \left\langle \frac{d\varphi_\sigma^a}{dx_\sigma^a} \middle| \frac{d\varphi_{\sigma'}^{a'}}{dx_{\sigma'}^{a'}} \right\rangle \frac{dx_\sigma^a}{dg_2} \frac{dx_{\sigma'}^{a'}}{dg_2}, \quad (\text{C6})$$

$$F_Q^\rho = \sum_a^{n_p} \sum_{a'}^{n_p} \sum_{\sigma=\pm} \langle \varphi_\sigma^a | \varphi_{\sigma'}^{a'} \rangle \frac{dc_\sigma^a}{dg_2} \frac{dc_{\sigma'}^{a'}}{dg_2}, \quad (\text{C7})$$

while the mixed terms are not vanishing due to the inter-polaron terms

$$F_Q^{\xi,x} = \sum_a^{n_p} \sum_{a' \neq a}^{n_p} \sum_{\sigma=\pm} \left(c_\sigma^a c_{\sigma'}^{a'} \left\langle \frac{d\varphi_\sigma^a}{d\xi_\sigma^a} \middle| \frac{d\varphi_{\sigma'}^{a'}}{dx_{\sigma'}^{a'}} \right\rangle \frac{d\xi_\sigma^a}{dg_2} \frac{dx_{\sigma'}^{a'}}{dg_2} + c_\sigma^a c_{\sigma'}^{a'} \left\langle \frac{d\varphi_\sigma^a}{dx_\sigma^a} \middle| \frac{d\varphi_{\sigma'}^{a'}}{d\xi_{\sigma'}^{a'}} \right\rangle \frac{dx_\sigma^a}{dg_2} \frac{d\xi_{\sigma'}^{a'}}{dg_2} \right), \quad (\text{C8})$$

$$F_Q^{\xi,\rho} = \sum_a^{n_p} \sum_{a' \neq a}^{n_p} \sum_{\sigma=\pm} \left(c_\sigma^a \frac{d\xi_\sigma^a}{dg_2} \left\langle \frac{d\varphi_\sigma^a}{d\xi_\sigma^a} \middle| \varphi_{\sigma'}^{a'} \right\rangle \frac{dc_{\sigma'}^{a'}}{dg_2} + \frac{dc_\sigma^a}{dg_2} \langle \varphi_\sigma^a | \frac{d\varphi_{\sigma'}^{a'}}{d\xi_{\sigma'}^{a'}} \rangle c_{\sigma'}^{a'} \frac{d\xi_{\sigma'}^{a'}}{dg_2} \right), \quad (\text{C9})$$

$$F_Q^{x,\rho} = \sum_a^{n_p} \sum_{a' \neq a}^{n_p} \sum_{\sigma=\pm} \left(c_\sigma^a \frac{dx_\sigma^a}{dg_2} \left\langle \frac{d\varphi_\sigma^a}{dx_\sigma^a} \middle| \varphi_{\sigma'}^{a'} \right\rangle \frac{dc_{\sigma'}^{a'}}{dg_2} + \frac{dc_\sigma^a}{dg_2} \langle \varphi_\sigma^a | \frac{d\varphi_{\sigma'}^{a'}}{dx_{\sigma'}^{a'}} \rangle c_{\sigma'}^{a'} \frac{dx_{\sigma'}^{a'}}{dg_2} \right). \quad (\text{C10})$$

Nevertheless, the intra-polaron terms in $F_Q^{\xi,x}$, $F_Q^{\xi,\rho}$, and $F_Q^{x,\rho}$ are still vanishing due to

$$\left\langle \frac{d\varphi_\sigma^a}{d\xi_\sigma^a} \middle| \frac{d\varphi_\sigma^a}{dx_\sigma^a} \right\rangle = \left\langle \frac{d\varphi_\sigma^a}{d\xi_\sigma^a} \middle| \varphi_\sigma^a \right\rangle = \left\langle \frac{d\varphi_\sigma^a}{dx_\sigma^a} \middle| \varphi_\sigma^a \right\rangle = 0, \quad (\text{C11})$$

$$\left\langle \frac{d\varphi_\sigma^a}{dx_\sigma^a} \middle| \frac{d\varphi_\sigma^a}{d\xi_\sigma^a} \right\rangle = \langle \varphi_\sigma^a | \frac{d\varphi_\sigma^a}{d\xi_\sigma^a} \rangle = \langle \varphi_\sigma^a | \frac{d\varphi_\sigma^a}{dx_\sigma^a} \rangle = 0. \quad (\text{C12})$$

As the inter-polaron overlaps in separate wave packets are relatively smaller, the intra-polaron terms are still playing a leading role. Note that $F_Q^{\xi,x}$, $F_Q^{\xi,\rho}$, and $F_Q^{x,\rho}$ only contain inter-polaron terms, while F_Q^ξ , F_Q^x , and F_Q^ρ are composed of larger intra-polaron terms and smaller inter-polaron terms. Furthermore, in a finite displacement the anti-polaron has much smaller weight due to the higher potential in a displacement direction opposite to the potential [30, 36]. As a result, the polaron contribution described in Appendix B is still playing a leading role. Thus, in the finite- Ω regime, we also have a diverging QFI from the different sensitivity resources qualitatively similar to the small- Ω regime, as one sees in Fig 5(d).

Appendix D: QFI by exact diagonalization

In the exact diagonalization the wave function is expanded in the Fock space

$$|\psi\rangle = |\psi_+\rangle + |\psi_-\rangle, \quad |\psi_\pm\rangle = \sum_{n=0}^{\infty} c_n^\pm |n\rangle \quad (\text{D1})$$

where n is the photon number and \pm labels the spin components. The Hamiltonian can be rewritten in a matrix form on the basis $|\pm, n\rangle$, the matrix of the mixed linear and nonlinear couplings with the bias field is provided

in Ref.[36]. In principle, the basis sums over all photon number, while a basis cutoff is applied in practice within the convergence in required precision. The derivative of the wave function with respect to the parameter λ is then determined by the variations of the basis weights c_n^\pm

$$|\psi'_\pm\rangle = \sum_{n=0}^{\infty} \frac{dc_n^\pm}{d\lambda} |n\rangle. \quad (\text{D2})$$

Then the QFI for a pure state is available by

$$\begin{aligned} F_Q(\lambda) &= 4 \left[\langle \psi'(\lambda) | \psi'(\lambda) \rangle - |\langle \psi'(\lambda) | \psi(\lambda) \rangle|^2 \right] \\ &= 4 \left(\sum_{n=0}^{\infty} \left| \frac{dc_n^\pm}{d\lambda} \right|^2 - \left| \sum_{n=0}^{\infty} \frac{dc_n^{\pm*}}{d\lambda} c_n^\pm \right|^2 \right) \end{aligned} \quad (\text{D3})$$

As mentioned in Sec. III, the $|\langle \psi'(\lambda) | \psi(\lambda) \rangle|$ term in $F_Q(\lambda)$ vanishes for a real wave function [43], which is exact and also can be checked numerically by the exact diagonalization via the second term in (D3) within the required numerical precision.

-
- [1] L. Garbe, M. Bina, A. Keller, M. G. A. Paris, and S. Felicetti, Phys. Rev. Lett. **124**, 120504 (2020).
- [2] V. Montenegro, U. Mishra, and A. Bayat, Phys. Rev. Lett. **126**, 200501 (2021).
- [3] Y. Chu, S. Zhang, B. Yu, and J. Cai, Phys. Rev. Lett. **126**, 010502 (2021).
- [4] L. Garbe, O. Abah, S. Felicetti, and R. Puebla, Phys. Rev. Research **4**, 043061 (2022).
- [5] T. Ilias, D. Yang, S. F. Huelga, M. B. Plenio, PRX Quantum **3**, 010354 (2022).
- [6] Z.-J. Ying, S. Felicetti, G. Liu, and D. Braak, Entropy **24**, 1015 (2022).
- [7] C. Hotter, H. Ritsch, and K. Gietka, Phys. Rev. Lett. **132**, 060801 (2024).
- [8] U. Alushi, W. Górecki, S. Felicetti, and R. Di Candia, Phys. Rev. Lett. **133**, 040801 (2024).
- [9] C. Mukhopadhyay and A. Bayat, Phys. Rev. Lett. **133**, 120601 (2024).
- [10] G. Mihailescu, A. Bayat, S. Campbell and A. K. Mitchell, Quantum Sci. Technol. **9**, 035033 (2024).
- [11] Z.-J. Ying, Adv. Quantum Technol. **7**, 2400288 (2024); *ibid.* **7**, 2470029 (2024).
- [12] P. Forn-Díaz, L. Lamata, E. Rico, J. Kono, and E. Solano, Rev. Mod. Phys. **91**, 025005 (2019).
- [13] A. F. Kockum, A. Miranowicz, S. De Liberato, S. Savasta, and F. Nori, Nature Reviews Physics **1**, 19 (2019).
- [14] H.-P. Eckle, *Models of Quantum Matter* (Oxford University, London, 2019)
- [15] J. Larson and T. Mavrogordatos, *The Jaynes-Cummings Model and Its Descendants*, IOP, London, (2021).
- [16] A. Le Boité, Adv. Quantum Technol. **3**, 1900140 (2020).
- [17] W. Qin, A. Miranowicz, P.-B. Li, X.-Y. Lü, J. Q. You, and F. Nori, Phys. Rev. Lett. **120**, 093601 (2018).
- [18] X.-F. Pan, P.-B. Li, X.-L. Hei, X. Zhang, M. Mochizuki, F.-L. Li, and F. Nori, Phys. Rev. Lett. **132**, 193601 (2024).
- [19] C. L. Degen, F. Reinhard, and P. Cappellaro, Rev. Mod. Phys. **89**, 035002 (2017).
- [20] L. Pezzè, A. Smerzi, M. K. Oberthaler, R. Schmied, and P. Treutlein, Rev. Mod. Phys. **90**, 035005 (2018).
- [21] L. Maccone and A. Ricciardi, Quantum **4**, 292 (2020).
- [22] B. J. Lawrie, P. D. Lett, A. M. Marino, and R. C. Pooser, ACS Photonics **6**, 1307 (2019).
- [23] K. Gietka and H. Ritsch, Phys. Rev. Lett. **130**, 090802 (2023).
- [24] A. Candeloro, S. Razavian, M. Piccolini, B. Teklu, S. Olivares, and M. G. A. Paris, Entropy **23**, 1353 (2021).
- [25] K. Gietka, C. Hotter, and H. Ritsch, Phys. Rev. Lett. **131**, 223604 (2023).
- [26] R. Horodecki, P. Horodecki, M. Horodecki, and K. Horodecki, Rev. Mod. Phys. **81**, 865 (2009).
- [27] O. Gühne and G. Tóth, Phys. Rep. **474**, 1 (2009).
- [28] J. Liu, M. Liu, Z.-J. Ying, and H.-G. Luo, Adv. Quantum Technol. **4**, 2000139 (2021).
- [29] S. Ashhab, Phys. Rev. A **87**, 013826 (2013).
- [30] Z.-J. Ying, M. Liu, H.-G. Luo, H.-Q. Lin, and J. Q. You, Phys. Rev. A **92**, 053823 (2015).
- [31] M.-J. Hwang, R. Puebla, and M. B. Plenio, Phys. Rev. Lett. **115**, 180404 (2015).
- [32] M.-J. Hwang and M. B. Plenio, Phys. Rev. Lett. **117**, 123602 (2016).
- [33] J. Larson and E. K. Irish, J. Phys. A: Math. Theor. **50**, 174002 (2017).
- [34] M. Liu, S. Chesi, Z.-J. Ying, X. Chen, H.-G. Luo, and H.-Q. Lin, Phys. Rev. Lett. **119**, 220601 (2017).
- [35] Z.-J. Ying, L. Cong, and X.-M. Sun, arXiv:1804.08128, (2018); J. Phys. A: Math. Theor. **53**, 345301 (2020).
- [36] Z.-J. Ying, Phys. Rev. A **103**, 063701 (2021).
- [37] Z.-J. Ying, Adv. Quantum Technol. **5**, 2100088 (2022); *ibid.* **5**, 2270013 (2022).
- [38] Z.-J. Ying, Adv. Quantum Technol. **5**, 2100165 (2022).
- [39] Z.-J. Ying, Adv. Quantum Technol. **6**, 2200068 (2023); *ibid.* **6**, 2370011 (2023).
- [40] Z.-J. Ying, Adv. Quantum Technol. **6**, 2200177 (2023); *ibid.* **6**, 2370071 (2023).
- [41] Z.-J. Ying, Phys. Rev. A **109**, 053705 (2024).
- [42] Z.-J. Ying, Adv. Quantum Technol. **7**, 2400053 (2024); *ibid.* **7**, 2470017 (2024).
- [43] Z.-J. Ying, W.-L. Wang, and B.-J. Li, Phys. Rev. A **110**, 033715 (2024).
- [44] Z.-J. Ying, arXiv:2411.10734 (2024).
- [45] R. Grimaudo, A. S. Magalhães de Castro, A. Messina, E. Solano, and D. Valenti, Phys. Rev. Lett. **130**, 043602 (2023).
- [46] R. Grimaudo, D. Valenti, A. Sergi, and A. Messina, Entropy **25**, 187 (2023).
- [47] R. Grimaudo, G. Falci, A. Messina, E. Paladino, A. Sergi, E. Solano, D. Valenti, Phys. Rev. Res. **6**, 043298 (2024).

- [48] C. Liu, and J.-F. Huang, *Sci. China Phys. Mech. Astron.* **67**, 210311 (2024).
- [49] G.-L. Zhu, C.-S. Hu, H. Wang, W. Qin, X.-Y. Lü, and F. Nori, *Phys. Rev. Lett.* **132**, 193602 (2024).
- [50] D. Braak, *Phys. Rev. Lett.* **107**, 100401 (2011).
- [51] D. Braak, Q.H. Chen, M.T. Batchelor, and E. Solano, *J. Phys. A Math. Theor.* **49**, 300301 (2016).
- [52] I. I. Rabi, *Phys. Rev.* **51**, 652 (1937).
- [53] E. Solano, *Physics* **4**, 68 (2011).
- [54] Q.-H. Chen, C. Wang, S. He, T. Liu, and K.-L. Wang, *Phys. Rev. A* **86**, 023822 (2012).
- [55] K. Gietka, *Phys. Rev. A* **105**, 042620 (2022).
- [56] X. Gu, A. F. Kockum, A. Miranowicz, Y. X. Liu, and F. Nori, *Phys. Rep.* **718-719**, 1 (2017).
- [57] Q.-T. Xie, S. Cui, J.-P. Cao, L. Amico, and H. Fan, *Phys. Rev. X* **4**, 021046 (2014).
- [58] J.-F. Huang, J.-Q. Liao, and L.-M. Kuang, *Phys. Rev. A* **101**, 043835 (2020).
- [59] J. Peng, J. Zheng, J. Yu, P. Tang, G. Alvarado Barrios, J. Zhong, E. Solano, F. Albarrán-Arriagada, and L. Lamata, *Phys. Rev. Lett.* **127**, 043604 (2021).
- [60] J. Peng, E. Rico, J. Zhong, E. Solano, and I. L. Egusquiza, *Phys. Rev. A* **100**, 063820 (2019).
- [61] Y. Wang, W.-L. You, M. Liu, Y.-L. Dong, H.-G. Luo, G. Romero, and J. Q. You, *New J. Phys.* **20**, 053061 (2018).
- [62] A. Stokes and A. Nazir, *Nat. Commun.* **10**, 499 (2019).
- [63] X. Chen, Z. Wu, M. Jiang, X.-Y. Lü, X. Peng, and J. Du, *Nat. Commun.* **12**, 6281 (2021).
- [64] G. Liu, W. Xiong, and Z.-J. Ying, *Phys. Rev. A* **108**, 033704 (2023).
- [65] L.-T. Shen, Z.-B. Yang, H.-Z. Wu, and S.-B. Zheng, *Phys. Rev. A* **95**, 013819 (2017).
- [66] K. K. W. Ma, *Phys. Rev. A* **102**, 053709 (2020).
- [67] E. K. Irish and A. D. Armour, *Phys. Rev. Lett.* **129**, 183603 (2022).
- [68] Z.-M. Li, D. Ferri, D. Tilbrook, and M. T. Batchelor, *J. Phys. A: Math. Theor.* **54**, 405201 (2021).
- [69] D. F. Padilla, H. Pu, G.-J. Cheng, and Y.-Y. Zhang, *Phys. Rev. Lett.* **129**, 183602 (2022).
- [70] W.-T. He, C.-W. Lu, Y.-X. Yao, H.-Y. Zhu, and Q. Ai, *Front. Phys.* **18**, 31304 (2023).
- [71] J. Zhang, Y.-L. Zhou, Y. Zuo, H. Zhang, P.-X. Chen, H. Jing, and L.-M. Kuang, *Adv. Quantum Technol.* **7**, 2300350 (2024).
- [72] Y. Yan, Z. Lü, L. Chen, and H. Zheng, *Adv. Quantum Technol.* **6**, 2200191 (2023).
- [73] S. Cheng, H.-G. Xu, X. Liu, and X.-L. Gao, *Physica A* **604**, 127940 (2022).
- [74] H.-G. Xu, V. Montenegro, X.-L. Gao, J. Jin, and G. D. de Moraes Neto, *Phys. Rev. Research* **6**, 013001 (2024).
- [75] U. Alushi, T. Ramos, J. J. García-Ripoll, R. Di Candia, and S. Felicetti, *PRX Quantum* **4**, 030326 (2023).
- [76] G. Lyu, K. Kottmann, M. B. Plenio, and M.-J. Hwang, *Phys. Rev. Research* **6**, 033075 (2024).
- [77] Z. Wu, C. Hu, T. Wang, Y. Chen, Y. Li, L. Zhao, X.-Y. Lü, and X. Peng, *Phys. Rev. Lett.* **133**, 173602 (2024).
- [78] J. E. Mooij, T. P. Orlando, L. Levitov, L. Tian, and C. H. van der Wal, S. Lloyd, *Science* **285**, 1036 (1999).
- [79] S. Felicetti, J. S. Pedernales, I. L. Egusquiza, G. Romero, L. Lamata, D. Braak, E. Solano, *Phys. Rev. A* **92**, 033817 (2015).
- [80] L. Duan, Y.-F. Xie, D. Braak, Q.-H. Chen, *J. Phys. A* **49**, 464002 (2016).
- [81] L. Garbe, I. L. Egusquiza, E. Solano, C. Ciuti, T. Coudreau, P. Milman, S. Felicetti, *Phys. Rev. A* **95**, 053854 (2017).
- [82] S. Felicetti, D. Z. Rossatto, E. Rico, E. Solano, and P. Forn-Díaz, *Phys. Rev. A* **97**, 013851 (2018).
- [83] L. Cong, X.-M. Sun, M. Liu, Z.-J. Ying, H.-G. Luo, *Phys. Rev. A* **99**, 013815 (2019).
- [84] R. J. Armenta Rico, F. H. Maldonado-Villamizar, and B. M. Rodriguez-Lara, *Phys. Rev. A* **101**, 063825 (2020).
- [85] P. Bertet, I. Chiorescu, C. J. P. M. Harmans, and J. E. Mooij, arXiv:cond-mat/0507290.
- [86] V. V. Mangazeev, M. T. Batchelor, and V. V. Bazhanov, *J. Phys. A: Math. Theor.* **54**, 12LT01 (2021).
- [87] Z.-M. Li and M. T. Batchelor, *Phys. Rev. A* **103**, 023719 (2021).
- [88] C. Reyes-Bustos, D. Braak, and M. Wakayama, *J. Phys. A: Math. Theor.* **54**, 285202 (2021).
- [89] E. K. Irish and J. Gea-Banacloche, *Phys. Rev. B* **89**, 085421 (2014).
- [90] S. L. Braunstein and C. M. Caves, *Phys. Rev. Lett.* **72**, 3439 (1994).
- [91] M. M. Taddei, B. M. Escher, L. Davidovich, and R. L. de Matos Filho, *Phys. Rev. Lett.* **110**, 050402 (2013).
- [92] M. M. Rams, P. Sierant, O. Dutta, P. Horodecki, and J. Zakrzewski, *Phys. Rev. X* **8**, 021022 (2018).
- [93] H.-Q. Zhou and J. P. Barjaktarevič, *J. Phys. A: Math. Theor.* **41** 412001 (2008).
- [94] S.-J. Gu, *Int. J. of Mod. Phys. B* **24** 4371, (2010).
- [95] W.-L. You, Y.-W. Li, and S.-J. Gu, *Phys. Rev. E* **76**, 022101 (2007).
- [96] W.-L. You and L. He, *J. Phys.: Condens. Matter* **27**, 205601 (2015).
- [97] P. Zanardi and N. Paunković, *Phys. Rev. E* **74**, 031123 (2006).
- [98] A. I. Lvovsky, *Photonics* Volume 1: Fundamentals of Photonics and Physics, pp. 121-164 Edited by D. Andrews, Wiley, West Sussex, United Kingdom, **2015**.
- [99] E. P. Wigner, *Phys. Rev.* **749**, 40 (1932).
- [100] J. Weinbub, D. K. Ferry, *Appl. Phys. Rev.* **5**, 041104 (2018).